Biomass and Bioenergy 170 (2023) 106730

Contents lists available at ScienceDirect

Biomass and Bioenergy

journal homepage: www.elsevier.com/locate/biombioe

Zr supported on non-acidic sepiolite for the efficient one-pot transformation of furfural into γ-valerolactone

Adrián García [a], Eleonora Monti [b,c], Alessia Ventimiglia [b,c], Nikolaos Dimitratos [b,c], Pablo J. Miguel [a], María Luisa López [d], Inmaculada Álvarez-Serrano [d], Tomás García [e], Maria Pilar Pico [f], Ana M. Dejoz [a], Benjamín Solsona [a,*]

[a] Departament d'Enginyeria Quimica, ETSE, Universitat de Valencia, Av. Universitat, Burjassot, Valencia, 46100, Spain
[b] Department of Industrial Chemistry "Toso Montanari", University of Bologna, Viale Risorgimento 4, Bologna, 40136, Italy
[c] Center for Chemical Catalysis- C3, Alma Master Studiorum Università di Bologna, Viale Risorgimento 4, Bologna, 40136, Italy
[d] Departamento de Química Inorgánica, Facultad de Ciencias Químicas, Universidad Complutense de Madrid, 28040, Madrid, Spain
[e] Instituto de Carboquímica (CSIC), C/Miguel Luesma Castán, 20018, Zaragoza, Spain
[f] Sepiolsa, Avenida del Acero, 14-16, Pol. UP-1 (Miralcampo), 19200, Azuqueca de Henares, Spain

ARTICLE INFO

Keywords:
One-pot
Sepiolite
Cheap supports
Wet impregnation
Zr dispersion

ABSTRACT

The growing demand of energy needs the search for alternative energy sources different to fossil fuels. The use of biomass as energy source is one of the most studied, because there are high value products that can be produced from biomass. One of these products is γ-valerolactone, that can be obtained from furfural, which is a biomass derived product. To transform furfural into γ-valerolactone is necessary a bifunctional catalyst and a hydrogen source. In this work, γ-valerolactone was obtained from furfural using 2-propanol as solvent and as hydrogen donor on Zr supported on sepiolite catalysts. It was demonstrated that sepiolite, which is a cheap material, can be used to develop efficient catalysts to produce high yields to γ-valerolactone from furfural in one-pot. The catalysts that presented the highest yield to γ-valerolactone were the ones with intermediate Zr-content (9–17 wt% ZrO_2). The highest TOFs have been obtained by those catalysts with Zr-loading up to 9 wt% ZrO_2, in which the ZrO_2 nanoparticles are well dispersed on the support and no formation of large clusters of ZrO_2 has been observed. Lewis and Brønsted acid sites are essential in the catalysts to produce the reactions to transform furfural into γ-valerolactone in one-pot, although in the present work, low concentration of Brønsted acid sites were observed in the catalysts. A possible positive role of basic sites to promote some intermediate steps has been also proposed. The catalytic results obtained are in the order of catalysts with Zr supported on zeolitic supports.

1. Introduction

The environmental problems and the energy crisis due to the use of fossil resources (limited, pollutant and non-renewable energy sources), have led to scientists to find other energy sources in the nature as a substitute of fossil fuels [1]. In the last years, there has been an increasing interest about the valorization of lignocellulosic biomass because it is a cheap renewable carbon source of energy [2,3]. Interestingly, it is possible obtaining valuable chemical products from agricultural residues, forestry wastes and energy crops without interfering with the food chain [4,5].

Lignocellulosic biomass can be degraded into their main components, lignin (15–25%), cellulose (40–50%) and hemicelluloses (20–35%). Hemicellulose can be transformed by depolymerization at high temperature and dehydrated in acidic medium into C5 and C6 monomers, mainly xylose. Xylose can be easily dehydrated through acid catalysis to produce furfural (FF) (Scheme S1) [6–11]. Different homogeneous acid catalysts such as H_2SO_4 have been studied to produce FF from C6 and C5 sugars, but separation and recovery problems exist. In the last years heterogeneous catalysts have been developed like resins, zeolites or metal oxides to produce FF to avoid these problems [11].

Furfural (FF) is a furan ring formaldehyde ($C_5H_4O_2$) with high value in the chemical and energy industry. It is mainly used as a solvent due to its aromatic and polar character [12–14]. Moreover, FF can be transformed into other value products such as γ-valerolactone (GVL), through a multiple steps route [15,16]. GVL can be used as a green solvent and it

* Corresponding author.
E-mail address: benjamin.solsona@uv.es (B. Solsona).

https://doi.org/10.1016/j.biombioe.2023.106730
Received 2 August 2022; Received in revised form 24 January 2023; Accepted 5 February 2023
Available online 19 February 2023

is a versatile compound for the synthesis of bio-fuels and chemicals (such as pentanediol, pentenoic acid or butadiene among others). GVL has a melting point of −31 °C, a boiling point of 207 °C and a high flash point (96 °C) and it has a very low toxicity. GVL can be transformed into liquid gasoline fuels using different types of catalysts as it has high combustion energy similar to the one corresponding to ethanol. However, it has an energetic density and cetane numbers lower than fossils fuels; therefore it has been studied more as an additive to fuels [17,18]. Moreover, it can be used as solvent to process the biomass, because it is able to dissolve biomass fractions avoiding the use of expensive solvents, enzymes or ionic liquids [19–21].

To transform FF into GVL several steps are required, two of them involving hydrogenation reactions. Firstly, FF is hydrogenated into furfuryl alcohol (FAL) or furfuryl ether (FE). Then, depending on the solvent used, FE is converted into alkyl levulinate, which is transformed into alkyl 4-hydroxy-pentanoate by another hydrogenation and, finally, to GVL by cyclization [22–29].

For the hydrogenation reaction it is necessary a hydrogen source to carry out these reactions. Alcohols have been used in many studies [30–32] as hydrogen source using the Meerwein-Ponndorf-Verley (MPV) reaction for the catalytic transfer hydrogenation. The most studied alcohols have been 2-propanol, 2-butanol or 2-pentanol, with which the highest yields to GVL were obtained.

In the recent years a wide range of metal-based catalysts have been designed with acid sites to transform FF into GVL. It has been widely reported that the presence of Lewis acid sites (LAS) and Brønsted acid sites (BAS) are necessary in the catalysts to obtain GVL from FF in one-pot. Thus, LAS are necessary in all catalytic step reactions, except to transform furfuryl ether (FE) into alkyl levulinate (AL) which requires the presence of BAS [21,33–35].

Several studies have used Zr supported on different materials such as plain and dealuminated zeolites, varying its LAS to BAS ratio, in order to catalyze selectively the transformation of FF into GVL. Zr has been reported to be one of the most active metals for the MPV reaction [36–38]. Bui et al. [33] achieved a 62% yield to GVL from FF in 2-butanol at 120 °C for 48 h using a physical mixture of catalysts: Lewis acidic Zr-Beta and Brønsted acidic Al-MFI-ns. The authors reported an easy way of controlling the BAS to LAS ratio, leading to the optimization of the catalytic performance. Similarly, Zhang et al. [31] designed a catalytic system consisting of two catalysts, Zr-HY and Al-HY, reaching a significant GVL yield (85% at 120 °C after 5 h) using 2-pentanol as the desired solvent. A combination of Au nanoparticles supported on ZrO_2 (catalyst with LAS) and ZSM-5 zeolite (BAS catalyst) was reported to achieve 80% of GVL yield at 120 °C after 30 h in 2-propanol [39].

In another work, Hernández et al. [40] reported a GVL yield of 23% in one-pot from FF using only one beta zeolitic catalyst. ZrO_2/SBA-15 catalysts have also demonstrated to be an interesting alternative catalytic system [41]. The use of dealuminated zeolites as supports for Zr has also shown an improved catalytic performance. For example, Melero et al. [42] synthesized a Zr catalyst supported on dealuminated beta zeolite, achieving 70% of GVL selectivity. In another study [43], heteropolyacids were used to modify the acidity of the surface of Zr-Beta catalysts. In this way, GVL yields of 70% were reached. In another work, Ye et al. [44] synthesized a bifunctional catalyst (HZSM-5-supported zirconium phosphate) leading to a GVL yield of 64.2%. Gao et al. [32] synthesized and tested Fe_3O_4 nanoparticles and ZrO_2-doped mesoporous MCM-41 as a monolithic multifunctional catalyst to transform FF with a GVL yield of 85% with iso-propanol.

Other non zeolitic catalysts have been also tested for the transformation of FF into GVL. Zhou et al. [45] synthesized Au-Ni nanoparticles supported on ZrO_2. These authors achieved a yield to GVL of 51.5% using formic acid as a green hydrogen source. Unfortunately, this reaction to take place required two steps. Also employing Au-containing materials, Morandi et al. [46] designed Au-Ru nanoparticles supported on ZrO_2 that could reach a yield to GVL of 71%.

Not only Zr can provide LAS but also other elements such as Al or Sn. In fact, Winoto et al. [47] designed a catalysts comprised of Sn supported on dealuminated beta zeolite achieving a yield of GVL up to 60%.

In the present article, we will show that sepiolite, a natural, cheap and readily available material, can be an effective support of Zr as efficient as in the case of using zeolites, leading to comparable yields to GVL. Additionally, it will be demonstrated that the FF transformation into GVL can take place with catalysts in which the amount of LAS is very low, avoiding the use of acidic or expensive supports. In this paper, Zr/sepiolite catalysts with different Zr-loadings have been prepared and tested in the one-pot transformation of FF into GVL, using 2-propanol as both solvent and hydrogen source.

2. Materials and methods

2.1. Preparation of catalysts

Zr was supported on raw sepiolite, which was collected from Toledo (Spain) and provided by Sepiolsa (Azuqueca de Henares, Spain). The composition of sepiolite is: sepiolite 97 wt%, dolomite: 1.9 wt%, other clays 1.1 wt%. Catalysts were synthesized by a wet impregnation method using water as a solvent. Different Zr concentrations were used by adding the appropriate amount of zirconium (IV) oxynitrate hydrate ($ZrO(NO_3)_2{\cdot}xH_2O$ (99% purity) from Sigma-Aldrich, St. Louis, MO, USA) in distilled water. When the desired amount of the Zr precursor was dissolved in the water, sepiolite was added and it was placed in a hot-plate stirrer at 80 °C under vigorous stirring until all the solvent was evaporated. Typically, for 1 g of sepiolite 10 mL of distillate water were used. The catalysts were labelled as xZrO_2/Sep, being x the final ZrO_2 content (2.5, 6.5, 9, 12, 17 and 29 wt% were synthesized). Finally, samples were dried at 100 °C for 12 h and later calcined at 500 °C in static air for 6 h.

For a proper comparison, raw sepiolite was also calcined at 500 °C in static air for 6 h.

2.2. Characterization techniques

Nitrogen adsorption-desorption was undertaken at 77 K and measured on a Micromeritics Tristar apparatus with enhanced secondary void system after outgassing at 423 K before reaching vacuum conditions. Brunauer-Emmett-Teller (BET) equations were used to determine the surface area.

Power X-ray diffraction (XRD) patterns of catalysts were collected at 2θ between 10 and 80 ° using an Enraf Nonius FR590 sealed tube diffractometer (Bruker, Delft, The Netherlands) equipped with a monochromatic Cu Kα1 source (40 kV and 30 mA).

High resolution transmission electron microscopy (HRTEM) analysis was performed using a JEOL JEM 2100F (200 kV) in order to analyze catalysts structure and morphology. In order to prepare the samples to be analyzed, the powders were crushed under n-butanol and dispersed them over copper grids covered with a holey carbon film. (Sepiolite fibers are not stable under the beam, therefore the analysis had to be fast and composition data should be taken as estimative.)

Fourier transform infrared spectroscopy (FTIR) analysis of samples was performed using a Cary 600 spectrometer (Agilent Technologies) with a resolution of 8 cm^{-1} and a scanning frequency of 32 min^{-1} at room temperature. Spectra were collected in the 4000-650 cm^{-1} region.

Ammonia thermal programmed desorption (NH_3-TPD) analysis was carried out with a Micromeritics Autochem II 2920 analyser in order to investigate the total acid strength and density of acidic sites. Around 100 mg of the samples were placed in a quartz tube and pre-treated with He with a flow of 20 mL min^{-1} of He at 500 °C for 2 h, then the temperature was decreased to 100 °C and exposed to a mixture of 10% NH_3 in He (20 mL min^{-1}) for 20 min. The sample was purged with He for 2 h after flushing. The NH_3 desorption was subsequently monitored using a thermal conductivity detector (TCD) at a heating rate of 10 °C/min up to 500 °C under He flow (20 mL min^{-1}).

CO_2-Temperature programmed desorption (CO_2-TPD) measurements were carried out in a fixed-bed flow reactor. 100 mg of the sample was pre-treated with He (50 ml min^{-1}) at 200 °C for 1 h. After cooling to 150 °C, CO_2 was introduced and adsorbed until saturation. Then, desorption was started at a heating rate of 10 °C min^{-1} in He (50 ml min^{-1}). The desorbed CO_2 was analyzed with a thermal conductivity detector (TCD).

The concentration of Lewis and Brønsted acid sites (LAS and BAS) was measured using Fourier transform infrared (FT-IR) after adsorbing pyridine as a probe molecule. FT-IR-pyridine analysis was done using a Bruker Vertex 70 instrument equipped with a Pike DiffusIR cell attachment and recorded by using an MCT detector after 128 scans and with a 4 cm^{-1} resolution in the region 4000–450 cm^{-1} to acquire in situ DRIFT spectra. Firstly, samples were pre-treated in a He flow (10 mL min-1) for 1 h at 300 °C. After the pretreatment, FT-IT spectra were acquired at four different temperatures (50, 100, 200 and 300 °C). Then, the samples were exposed to a pyridine vapour (1 μL) at 50 °C for 20 min, followed by re-evacuation at 50–300 °C and IR spectra were collected at the different temperatures (50, 100, 200 and 300 °C).

The samples were analyzed by X-ray photoelectron spectroscopy (XPS) using a Kratos Axis ultra DLD photoelectron spectrometer with a non-monochromatized Mg Kα X-ray source ($h\nu = 1253.6$ eV). For survey scans and detailed scans an analyzer pass energy of 50 eV and 20 eV were used, respectively. Binding energies were taken to the C1s peak from adventitious carbonaceous contamination which was assumed to have a binding energy of 284.8 eV. XPS data were analyzed using CasaXPS software. A Gaussian–Lorentzian shape function was used to fit all the peaks of the corrected spectra. Iterations were performed using the Marquardt method. Relative standard deviations have been determined and it has been found that they were always below 1.5%.

2.3. Catalytic tests and analysis

An autoclave reactor was used to carry out the hydrogenation experiments. The internal part of the reactor was covered by a Teflon container of 25 mL, which fits with the steel walls. In a typical run, 0.25 mmol of FF were mixed with 5 mL of 2-propanol and 0.2 g of catalyst was added. The autoclave was purged with N_2 three times in order to remove the oxygen and was sealed. Then it was placed in a silicon bath at 180 °C and stirred at 800 rpm for the duration of the experiments (typically for 5 h), and later it was cooled in an ice-bath. The liquid products were collected by filtration for the quantitative analysis.

The reactants and products were analyzed by a gas chromatograph (GC), using a mod. 5890 GC instrument (Hewlett Packard, Palo Alto, CA, USA). The GC has an Agilent HP-1 column (30 m × 0.32 mm x 0.25 μm) and a flame ignition detector (FID) at 240 °C, and an injection port at 220 °C. The temperature program for the chromatographic cycle was as follows: (i) 35 °C isothermal for 30 min, (ii) a heating rate of 1.5 °C min^{-1} from 35 to 230 °C and (iii) 230 °C isothermal for 30 min. To identify other reaction by-products a gas chromatography-mass spectrometer was used (GC-MS5977A MSD-7890A, Agilent, Santa Clara, CA, USA). The temperature program used was the same as used in the GC-FID.

2.4. Recycle of catalysts

For the recycling test, a reaction with 0.5 g of catalyst was carried out. After the completeness of the reaction, solid catalyst was recovered by filtration and it was dried at 180 °C for 12 h in order to be used for the next cycles. For the second cycle of reaction 0.2 g of the spent catalyst was used for the reaction. The same procedure was done for carrying out the third cycle of reaction, e.g. 0.2 g of the spent catalyst of the second cycle was used to carry out the reaction.

3. Results

3.1. Characterization results: surface area and basic/acidic characteristics of the synthesized catalysts

Table 1 shows some physicochemical properties of the supported ZrO_2/Sep catalysts. Bare uncalcined sepiolite presents a high surface area of 320.5 m^2/g, that decreases until 160 m^2/g when is calcined. On the other hand, pure ZrO_2 presents a lower surface area of 54.5 m^2/g. As expected, the addition of Zr to the support, leads to a decrease of the surface area compared to that of sepiolite. When 2.5 % wt. of ZrO_2 is added, the surface area hardly decreases until 156.9 m^2/g. Further increase of the amounts of ZrO_2 (6–12 wt% ZrO_2) are accompanied with a drop of the surface area, until ca. 125 m^2/g. Finally, the sample with the highest amount of ZrO_2 added (29 % wt.) presented the lowest surface area (117 m^2/g).

The total acidity and basicity of these catalysts was estimated through temperature programmed desorption of NH_3 and CO_2, respectively. As it is shown in Table 1, the pure calcined sepiolite support presents acidic sites. Moreover, as expected the amount of acid sites increases when higher amounts of ZrO_2 are added to the support. If the acidity is normalized per surface area, it is evident that the increase of acidity observed is related to the amount of zirconium added. The acidity of sepiolite and pure ZrO_2 is not high, which means that adding Zr into the support creates new weak and medium strength acid sites, increasing the total acidity of their parent materials (pure ZrO_2 and sepiolite) (Fig. 1). Overall, it is observed that the presence of Zr is the main contributing factor for obtaining acidity. Then, although the amount of ammonia adsorbed increases with the Zr-loading, if this consumption is normalized per the amount of Zr, it is observed that the number of acidic sites per Zr sites is highest for those catalysts with the lowest Zr-loading.

The basicity of the catalysts was measured using CO_2-TPD and the results are shown in Fig. 2. For the uncalcined sepiolite support (Fig. S1), two broad peaks can be found in the 100–250 °C temperature range (related to the adsorption of surface OH– groups) and 300–500 °C (strong basic sites Mg–O–Mg, Mg–O–Si, *etc.*). However, when this sample is calcined the basicity is drastically reduced, likely due to the loss of water and (-OH) groups [48]. The addition of Zr led to an increase of the amount of basic sites compared to the calcined sepiolite (Table 1 and Fig. 2). For the samples with impregnated Zr, two desorption broad bands have been observed at ca. 240 and ca. 400 °C. These bands correspond to weak and medium basic sites, respectively. Significantly, both types of basic sites increased with the amount of Zr, being maximized for the sample with 17 wt% ZrO_2. At higher Zr loading (29 wt% ZrO_2), whilst weak basic sites were significantly reduced, medium basic sites were kept at comparable values, indicating that higher basicity strength is expected for this sample. Overall, a subtle shift of the first band towards higher temperatures is observed at higher Zr loadings (ca. 280 °C) compared to the sample with low Zr-loading (6.5Zr/Sep), indicating higher strength [48]. This increased basicity strength when adding Zr has been observed in other similar study with Zr supported on β-zeolite catalysts [49].

As for the reaction studied is of paramount importance the type of acidic sites, therefore, FTIR spectroscopy of adsorbed pyridine experiments were carried out. Through this technique the presence of Lewis acid sites (LAS) or Brønsted acid sites (BAS) can be distinguished (Fig. 3). The existence of coordinately bonded pyridine at LAS appears at adsorption bands at 1445, 1575 and 1600 cm^{-1} [50]. As pyridine is desorbed when temperature increases, the intensity of these peaks is lower at higher temperatures. The presence of coordinately bonded pyridine at BAS can be related with absorption bands at 1550 and 1640 cm^{-1} [49]. Calcined sepiolite was analyzed by FTIR and no adsorption bands related with BAS or LAS were detected in any spectra at the different evacuation temperatures. All the catalysts presented adsorption bands related with the presence of LAS. This intensity of LAS is

Table 1
Physicochemical properties of Zr-supported catalysts, sepiolite and pure ZrO_2.

Sample	S_{BET} (m^2/g)	Acidity [mmol NH_3/g]	Acidity (μmol NH_3/m^2)	Acidity per ZrO_2 (mmol NH_3/g_{ZrO2})[b]	Basicity [mmol CO_2/g]	Basicity [μmol CO_2/m^2]	Basicity per ZrO_2 (mmol CO_2/g_{ZrO2})[b]	Basic/Acid sites
Sepiolite[a]	160.1	20.1	109	–	0.5	3.0	–	0.024
2.5ZrO_2/Sep	156.9	127.9	815	4312	4.9	30.9	176	0.038
6.5ZrO_2/Sep	128.0	173.4	1355	2555	5.4	42.2	81.7	0.031
9ZrO_2/Sep	126.5	174.3	1378	1713	6.2	49.0	63.3	0.035
12ZrO_2/Sep	125.3	191.9	1532	1432	5.7	45.5	43.3	0.031
17ZrO_2/Sep	119.2	219.4	1841	1172	7.5	62.6	41.2	0.034
29ZrO_2/Sep	117.0	324.1	2770	1048	7.1	60.9	22.8	0.022
ZrO_2	54.5	78.2	1435	78.2	1.9	34.4	1.9	0.023

[a] Sepiolite calcined in the same way that the Zr-catalysts (500 °C in air).
[b] Values determined per ZrO2 present in the catalyst (extracting that of the sepiolite support).

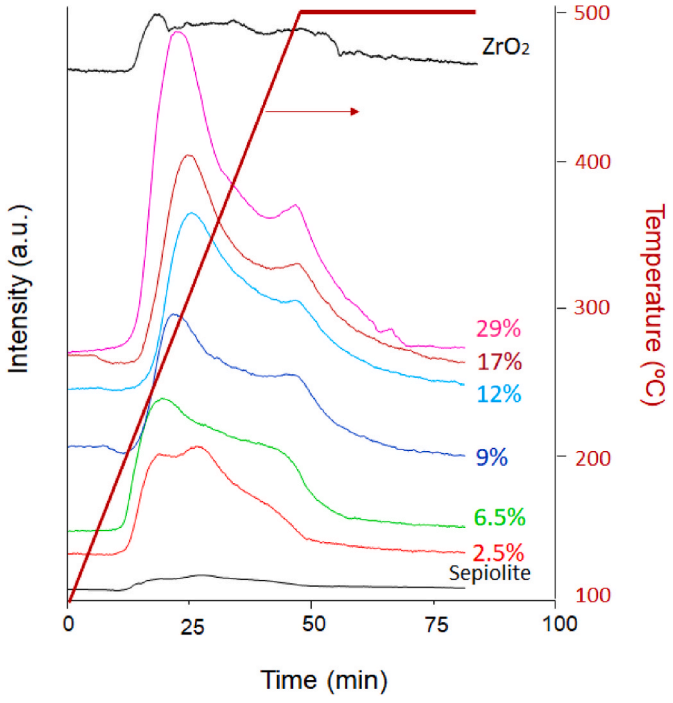

Fig. 1. NH_3-TPD profiles of the xZrO_2/Sep catalysts, pure ZrO_2 and pure sepiolite.

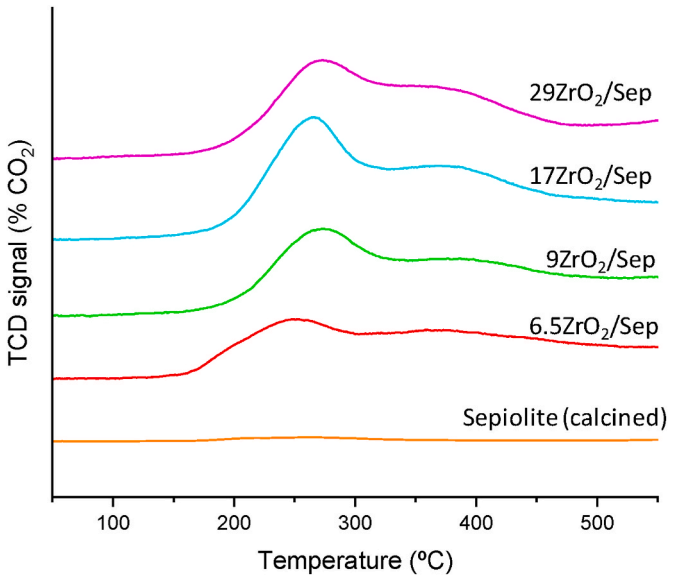

Fig. 2. CO_2-TPD profiles of representative catalysts.

higher when higher amounts of ZrO_2 are added [31]. The presence of BAS (especially by the peak at 1550 cm^{-1}) cannot be neglected for catalysts with ZrO_2-loadings of 9 wt% and higher (catalyst 9ZrO_2/Sep and 29ZrO_2/Sep), although, if present, the concentration is very low. The presence of BAS in these materials could be generated by the presence of OH-groups that, together with the LAS from Zr, originates those BAS, as proposed by Saito et al. [51].

3.2. Characterization results: XRD, FTIR and DR-UV-Vis

In order to know the crystallinity and structure of the synthesized samples, XRD analysis was carried out (Fig. 4). After calcination, sepiolite suffers a modification in its structure due to the loss of water. A phase change occurs due to the loss of the bound of H_2O, which produces a rotation of the phyllosilicate ribbons [52]. This leads to a change in the XRD pattern of sepiolite (Fig. S2). The XRD patterns of Zr-supported catalysts are very similar among them and also very similar to the reference calcined sepiolite. The only appreciable difference lies on the intensity, as a decrease was observed when the amount of ZrO_2 in the catalyst increases. Interestingly, peaks of ZrO_2 were no detected in any Zr/sepiolite catalysts, which suggests that maybe ZrO_2 nanoparticles are very small or ZrO_x species are well dispersed on the support. No diffraction peaks corresponding to mixed Zr-Si-phases or Zr-Mg-phases could be neither detected. On the other hand, bulk ZrO_2 catalyst presents good crystallinity, with the main diffraction peaks (2θ = 28.1°, 31.6° and 50.3°) corresponding to ZrO_2 in its monoclinic form (JCPDS: 37–1484) [53]. Additionally, reflections corresponding to tetragonal ZrO_2 (JCPDS 88–1007) at 2θ = 30.2°, 34.5° and 51° were also identified.

Fig. S3 shows FTIR spectra of the samples. The spectrum of raw sepiolite shows different peaks, which are characteristic of natural sepiolite. Bands from 3500 to 3200 cm^{-1} correspond to hydroxyl groups (-OH) and adsorbed water vibrations, bands from 1700 to 1600 cm^{-1} correspond to symmetric and asymmetric stretching of the crystal and zeolitic waters. These bands are associated at water disappearance when the sample is calcined, therefore these bands cannot be observed in the rest of the catalysts and in the calcined sepiolite. Peaks from 1000 cm^{-1} to 900 cm^{-1} corresponds to silicates (Si-O-Si), peaks from 750 cm^{-1} to 600 cm^{-1} correspond to magnesium hydroxides and finally, peaks at 450 cm^{-1} are related to Si-O-Mg of the octahedral-tetrahedral linkage [54–56]. The spectra of pure ZrO_2 present a peak at 750 cm^{-1}, which is attributed to Zr-O stretching vibrations at ZrO_2 [57]. A very low

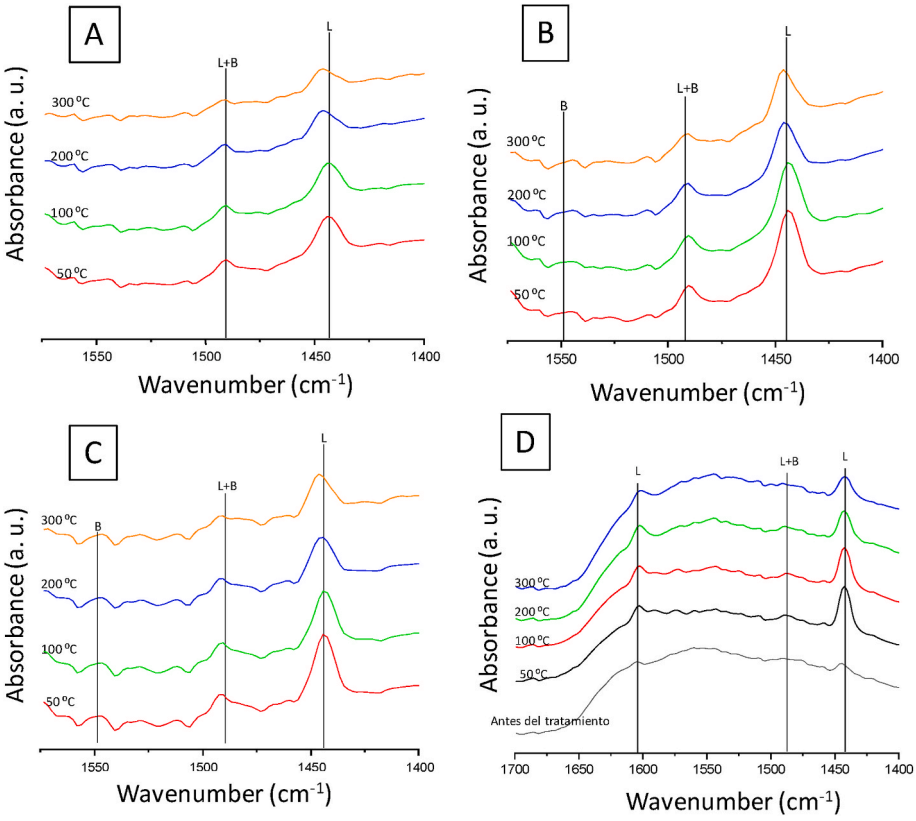

Fig. 3. FTIR spectra of pyridine absorbed at different temperatures over (A) 2.5ZrO_2/Sep, (B) 9ZrO_2/Sep, (C) 29ZrO_2/Sep y (D) ZrO_2. L: Lewis acid sites and B: Brønsted acid sites.

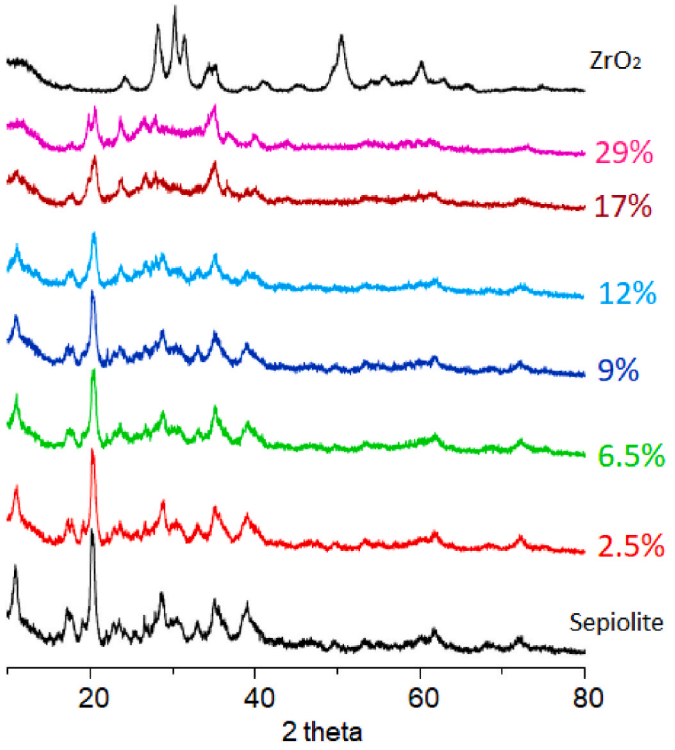

Fig. 4. XRD patterns of the support, catalysts and pure ZrO_2 after calcination.

intensity peak from 1700 cm^{-1} to 1600 cm^{-1} was observed and it corresponds to adsorbed water (Zr-H_2O). In the xZrO_2/Sep samples, additional peaks (from 4000 to 3000 and 1700 cm^{-1}) were observed and correspond to the crystal and zeolitic water but in lower intensity than in sepiolite. Moreover, the peaks associated to silicates (from 1000 cm^{-1} to 900 cm^{-1}) were observed in all samples, but when higher amounts of ZrO_2 were added to sepiolite, the intensity of the peaks was lower.

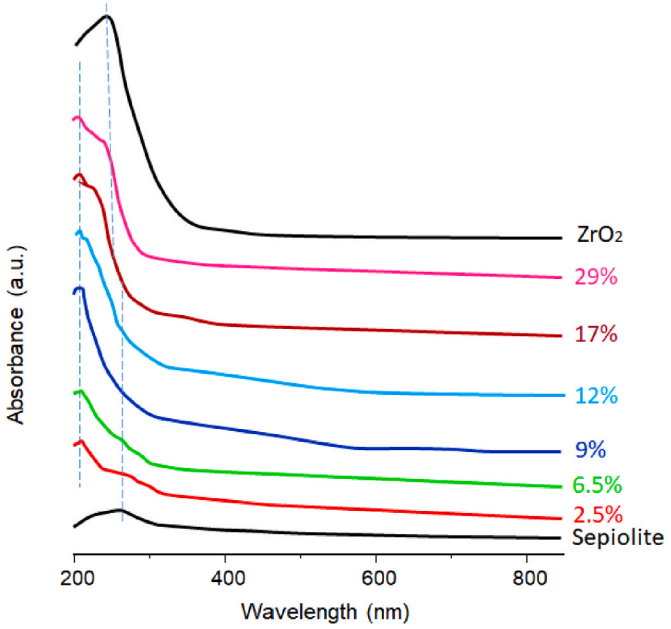

Fig. 5. DR-UV-vis spectra of catalysts compared with sepiolite and pure ZrO_2.

Samples were analyzed by DR-UV-vis to investigate the nature of Zr sites in the support (Fig. 5). Pure ZrO_2 catalysts shows two main bands, a high intensity peak at 230 nm with a shoulder at ca. 290 nm, typical of Zr-O-Zr charge transfer of ZrO_2 clusters [58–60]. A band around 203 nm is observed in all the Zr-containing catalysts, which is attributed to the ligand-to-metal charge transfer from O^{2-} to tetrahedral Zr^{4+}. This indicates that Zr is highly dispersed with a tetrahedral coordination on the support. For catalysts with high Zr-loadings (those with 17 and 29 wt% ZrO_2) these two bands at ca. 200 and 230 nm are observed, indicating that two different species (dispersed and aggregated ZrO_2 clusters) are co-existing on the surface of these samples. Catalysts with low Zr-loading (2.5 and 6 wt% ZrO_2) present also two different bands, at ca. 200 nm (tetrahedral Zr^{4+} species) and ca. 270 nm (band observed for pure sepiolite support).

3.3. Transmission electron microscopy results

HR-TEM analysis was carried out in order to analyze the structure and morphology of the catalysts. Fig. 6 shows TEM images of pure ZrO_2 and catalysts with low, medium and high Zr-loading (2.5ZrO_2/Sep, 9ZrO_2/Sep and 29ZrO_2/Sep). Fig. 6a and b shows the images for pure ZrO_2. Particles present pseudospherical shape with diameters ranging between 10 and 25 nm. The inset shows the corresponding ED pattern, which could be properly indexed considering the coexistence of tetragonal and monoclinic symmetries. The presence of nanovesicles is confirmed, as expected from hydrothermal routes of synthesis. The small particles appear aggregated leading to formations of different particle size up to ca. 50 nm. The coexistence of both symmetries is not rare in nanoparticulated ZrO_2, as previously reported [61]. High magnification images of particles show the contrasts indicating the interplanar distances indexed on the basis of monoclinic symmetry.

In Fig. 6c TEM images of the 2.5ZrO_2/Sep catalyst are shown. This catalyst presents a clear fiber morphology. These fibers present a variable size in a way that the width ranges between 10 and 30 nm and the length between 200 and 500 nm. Over the fibers, small dark spots are observed (smaller than 2 nm) likely corresponding to tiny ZrO_2 nanoparticles. EDs pattern (inset) indicates that particles remain at the nanoscale whereas the EDX spectrum (inset) shows that the zirconia particles are supported on the sepiolite but their distribution over the fibers is somewhat heterogeneous. Several EDX spectra on different regions give average compositions between 1.5 and 4% of ZrO_2, in good agreement with the actual loading.

For the 9ZrO_2/Sep catalyst (Fig. 6d), it can be observed that the impregnation method led to well distributed zirconia particles over the

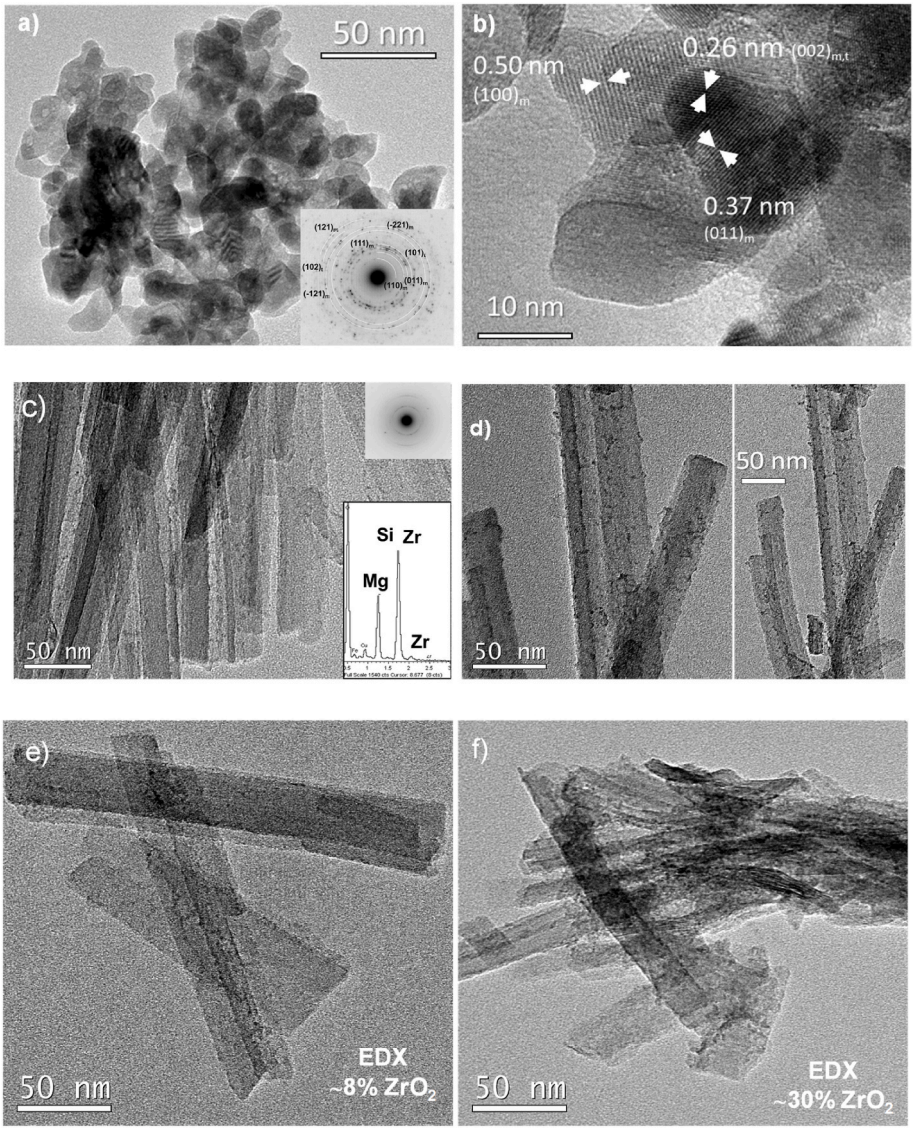

Fig. 6. TEM images of ZrO_2 (a, b) catalysts 2.5ZrO_2/Sep (c), 9ZrO_2/Sep (d) y 29ZrO_2/Sep (e, f).

sepiolite fibers. Indeed, EDX spectra over different regions are coherent with the expected composition, within the experimental semi-quantitative nature of the exploration. Thus, EDX on different areas gave a Zr-loading in all cases around 9 wt% ZrO_2, demonstrating the homogeneity of this catalyst. ZrO_2 particles observed over the sepiolite fibers were very well defined and, also, very tiny, in all cases with sizes below 2 nm.

Unlike the former catalyst, the $29ZrO_2$/Sep catalyst, did not show a homogeneous ZrO_2 distribution, due to the high nominal loading. Thus, by HRTEM images and EDX spectra in different regions of the sample a great degree of heterogeneity in the particle size distribution was observed (Fig. 6e and f). Thus, two different patterns are clearly seen. In several regions the sepiolite fibers are slightly covered (typical ZrO_2 loading of 5–10%) whereas other regions (majority) contain mass compositions of zirconia of 30–40%. Overall, the experimental semi-quantitative Zr-loading observed by TEM (ca. 25%) is slightly lower than that of the theoretical content according to the preparation method.

The surface chemistry of the catalysts, focusing on ZrO_2 nanoparticles was studied by XPS. Fig. S4 shows the fitted spectra of Zr 3d spin-orbit doublet peaks of four representative samples. For each sample, Zr 3d peaks are fitted with four contributions, corresponding to Zr-O-Zr (182.1 eV) and Zr-O-H (183.2 eV) species in ZrO_2 nanoparticles. Zr $3d_{5/2}$ and Zr $3d_{3/2}$ energy separation for each species is 2.4 eV, which is in line with literature data [62]. The relative contribution of each specie to the Zr 3d peak is reported in Table 2, showing that the contribution of hydroxyl species linked to Zr atoms is maximized for the sample with 9 wt% Zr loading, which was the catalyst where the best ZrO_2 dispersion was achieved. According to the chemical analysis of the surface (Table 2), the Zr-loading concomitantly increases with the Zr-loading until 9 wt% Zr. Until that content the amount of Zr is higher in the surface than in the bulk. However, in the samples with the highest Zr-loading the concentration of Zr increases less than that the composition suggests, confirming a decrease of the dispersion of Zr on the sepiolite surface.

3.4. Catalytic results

The synthesized catalysts have been tested in the transformation of furfural in the liquid phase. Firstly, the reaction was carried out with different supported catalysts, sepiolite and pure ZrO_2, as it was done in a previous work [63]. Table 3 shows the catalytic results obtained, including the yields to the main reaction product (γ-valerolactone GVL) as well as some other products detected such as isopropyl levulinate (IPL), furfuryl alcohol (FAL), furfuryl ether (FE) and levulinic acid (LA). Sepiolite, either fresh or calcined, showed not even traces of GVL and a low FF conversion was observed (<20%). Pure ZrO_2 showed a conversion of 98%, but without forming GVL and the main product was FAL (Fig. 7). Interestingly, all the Zr catalysts supported on sepiolite catalysts led to the formation of GVL with yields exceeding 15%. The highest yield to GVL under these reaction conditions was achieved by the catalysts with intermediate Zr-loadings (between 9 and 17 wt% ZrO_2), especially by the $9ZrO_2$/Sep sample. In the case of the IPL, the yield decreased when the amount of Zr-content of the catalyst increased. Very low yields to FAL were detected in all cases, probably because it rapidly reacts with 2-propanol to produce FE. Conversely to GVL, the FE formation presented a minimum at intermediate Zr-contents (see Fig. 8).

Overall, those catalysts with intermediate loadings have obtained the highest GVL yield. Additional experiments using low catalyst mass and low reaction times have been undertaken in order to determine the TOF values. As can be seen in Table 4, the catalytic activity was the highest using the catalyst with 12 wt% ZrO_2 although the turnover frequency decreased when the Zr-loading increased. Then, the dispersed Zr-species led not only to the increase in the relative amount of Zr on the surface of the catalyst but also presented an enhanced reactivity per Zr surface site.

4. Discussion

Zr supported on sepiolite can efficiently transform furfural into γ-valerolactone with high yields. It has been demonstrated that the presence of both Zr and the sepiolite support is necessary to obtain, in these reaction conditions, γ-valerolactone, since pure ZrO_2 or pure sepiolite cannot produce alone this lactone (not even traces have been detected). The highest yield to γ-valerolactone from furfural was achieved by those catalysts with an intermediate Zr-loading, ranging from 9 to 17 wt%.

The overall FF to GVL reaction has been reported to require both types of acid sites (Lewis and Brønsted) although in the present article high yield to GVL has been obtained with low proportion of Brønsted acid sites. We have observed that both the amount of acidic and basic sites increases when the amount of Zr increases. However, the number of basic sites is just 2–4% that of acidic sites (Table 1). Interestingly, the least efficient catalysts to GVL are those with the lowest proportion of basic sites (pure ZrO_2, pure sepiolite and $29ZrO_2$/sep), especially weak basic sites. The role of basicity in the general multistep mechanism to get GVL from FF is not well defined. It has been reported that a basic oxide as MgO enhances the hydrogenation of furfural [64] although the presence in the media of a strong basic compound such as NaOH blocks active sites from the catalyst. Then, the presence of weak basicity can be positive for the hydrogenation of FF to furfuryl alcohol [30,64], which is a clear intermediate for the overall reaction. Similarly, Li et al. [65] observed an enhanced reaction rate in the transformation of FF to FAL when the ratio of acid/basic sites was high (3.8–4). Moreover, Li et al. observed that a suitable acidity/basicity ratio promotes the selective production of FA from FF regardless of the BAS/LAS ratio [65]. Another possible advantage of the basic sites is their role in the decrease of side reactions that form by-products, which are not the typical intermediates for GVL formation. Moreover, basic sites can prevent the levulinic acid formation from furfuryl alcohol [30,64]. Rao et al. [49] suggest that both Lewis acid sites and basic sites are essential for a suitable catalytic transfer hydrogenation in the FF to GVL transformation. Other studies demonstrated that catalysts with moderated basicity could produce high yield to GVL from LA and its esters [66]. In these studies, it was demonstrated that basic sites with the aid of LAS can synergistically activate the dissociation of the hydroxyl groups in IPL for MPV reaction to produce 4-hydroxypentanoate and finally produce GVL by intramolecular esterification or transesterification [67]. Considering the results obtained in the present article, those catalysts that lead to the highest yield to GVL presents a ratio between basic and acid sites of

Table 2
Composition and XPS data of Zr/Sepiolite catalysts.

Catalyst	Zr-O-Zr		Zr-O-H		XPS Zr	Zr/Si XPS	Zr/Si bulk ICP	Ratio Zr[a]
	Zr 3d 5/2	Zr 3d 7/2	Zr 3d 5/2	Zr 3d 7/2				surface/bulk
	BE, ev (%area)	BE, ev (%area)	BE, ev (%area)	BE, ev (%area)	ox state			
$2.5ZrO_2$/Sep	182.1 (28.5)	184.5 (18.7)	183.1 (31.7)	185.5 (20.9)	Zr^{4+} (100%)	0.025	0.018	1.4
$9ZrO_2$/Sep	182.2 (26.4)	184.6 (17.4)	183.2 (33.8)	185.6 (22.2)	Zr^{4+} (100%)	0.082	0.070	1.2
$17ZrO_2$/Sep	182.2 (35.7)	184.6 (23.5)	183.2 (24.6)	185.6 (16.2)	Zr^{4+} (100%)	0.101	0.144	0.69
$29ZrO_2$/Sep	182.2 (33.9)	184.6 (22.3)	183.2 (26.4)	185.6 (17.4)	Zr^{4+} (100%)	0.150	0.289	0.52

[a] (Zr/Si by XPS)/(Zr/Si bulk).

Table 3
Furfural conversion and yield to products using Zr/sepiolite catalysts, sepiolite and pure ZrO_2.[a]

Catalyst	Conversion of FF (%)	Yield to GVL (%)	Yield to IPL (%)	Yield to FAL (%)	Yield to FE (%)	Others (%)	GVL Selectivity (%)
Raw Sepiolite	18.9	0	7	0	0	11.9	0
Sepiolite[b]	7.8	0	3.1	0	0	4.7	0
2.5ZrO_2/Sep	≥98	19.1	25.4	0.3	38.6	16.4	19.1
6.5ZrO_2/Sep		40.7	17.2	0.7	23.2	17.6	40.9
9ZrO_2/Sep		50.6	13.4	0.6	20.3	15	50.7
12ZrO_2/Sep		50.3	13.7	0.7	13.8	20.9	50.6
17ZrO_2/Sep		48.8	9.6	0.7	17.7	23	48.9
29ZrO_2/Sep		20.4	4.9	0.8	57.7	16	20.4
ZrO_2		0	0	93.6	3	3	0

[b] Sepiolite calcined as the Zr/sepiolite catalysts.
[a] Reaction condition: 0.25 mmol of furfural in 5 mL of 2-propanol, 0.2 g of catalyst, at 180 °C for 5 h.
[b] γ-valerolactone (GVL); isopropyl levulinate (IPL); furfuryl alcohol (FAL); furfuryl ether (FE); levulinic acid (LA).

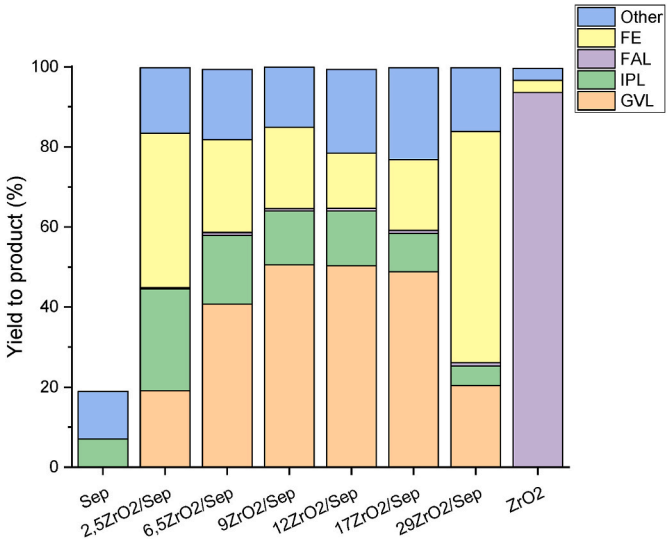

Fig. 7. One-pot production of GVL from FF with sepiolite, pure ZrO_2 and different catalysts. Reaction conditions: 0.25 mmol of FF in 5 mL of 2-propanol, 0.2 g of catalyst, for 5 h at 180 °C.

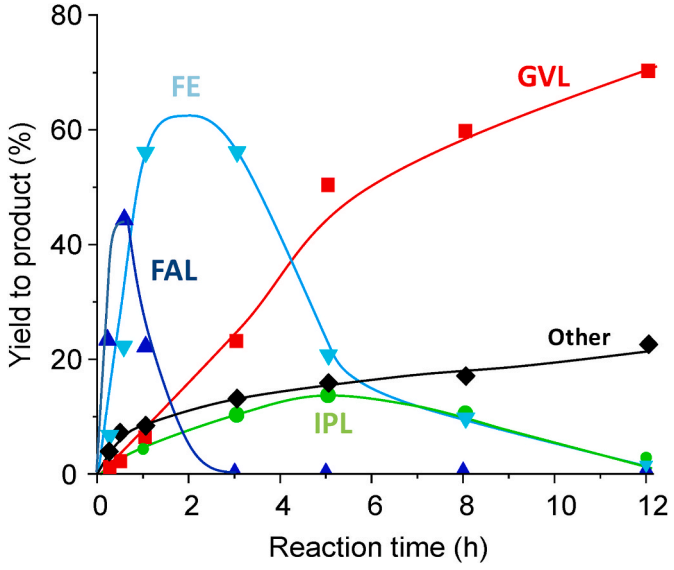

Fig. 8. Evolution of the yield to the different reaction products obtained from furfural using 9ZrO_2/Sep catalyst. Reaction condition: 0.25 mmol of furfural in 5 mL of 2-propanol, 0.2 g of catalyst, at 180 °C. Symbols: γ-valerolactone (GVL, ■); isopropyl levulinate (IPL, ?); furfuryl alcohol (FAL ▲); furfuryl ether (FE, ?) and other products (?).

0.03–0.04 and a prevalence of weak basic sites due to the presence of hydroxyl groups at the catalyst surface.

Additionally, the presence of Brønsted acid sites has been widely reported to be required for this reaction, especially for the FE to IPL conversion, although also play a role in the FAL to FE and in the IPL to GVL steps. According to the IR-Py results, it is possible the presence of Brønsted acid sites in the Zr supported on the sepiolite catalysts, regardless of the absence of BAS in the sepiolite and in the pure ZrO_2. BAS may have been generated by the interaction of the OH- groups of fresh sepiolite (before calcination) with the LAS of the Zr sites, as reported previously with other supports [51,63].

The evolution of the catalytic performance as a function of reaction time over 9ZrO_2/Sep catalyst has been studied in order to investigate and propose a simplified reaction scheme (Scheme 1). After only 15 min of reaction, the FF conversion exceeds 30%, with furfuryl alcohol being the predominant reaction product whereas γ-valerolactone was hardly formed. After 1 h, the furfural conversion reached 90%, furfuryl alcohol and furfuryl ether being the majority products (yields of 22 and 56%, respectively). However, the yield to γ-valerolactone was still only 6%. After 3 h of reaction, complete conversion of the furfural was observed and the yield to γ-valerolactone was increased until 30%. The yield to FE barely varied whereas that of FAL decreased and that of IPL increased. After 5 h, the yield to GVL was further increased until 50% whereas that of FE clearly diminished. After 8 h, the yield to GVL continued rising until 57% and, after 12 h, reached 70%. Moreover, another important product obtained was IPL. The maximum yield to IPL was obtained after

Table 4
Catalytic parameters in the furfural transformation on Zr catalysts supported on sepiolite.[a]

Catalyst	Furfural conversion (%)	Catalytic activity[b]	Specific activity[c]	TOF[d]
6.5ZrO_2/Sep	7.6	7.6	5.94	14.4
9ZrO_2/Sep	10.7	10.7	8.46	14.7
12ZrO_2/Sep	11.0	11.0	8.78	11.3
17ZrO_2/Sep	6.9	6.9	5.79	5.0
29ZrO_2/Sep	7.5	7.5	6.41	3.2
ZrO_2	6.9	6.9	12.7	0.9

[a] Reaction conditions: 5 mL of 2-propanol, 0.25 mmol of FF, 0.01 g of catalyst, 180 °C, reaction time = 0.25 h.
[b] Catalytic activity per gram of catalyst in 10^{-3} mol_{FF} h^{-1} g_{cat}^{-1}.
[c] Specific activity is the catalytic activity normalized per surface area in 10^{-5} mol_{FF} $h^{-1}m^{-2}$.
[d] Catalytic activity per mol of surface Zr present in the catalyst in mol_{FF} h^{-1} mol_{Zr}^{-1}.

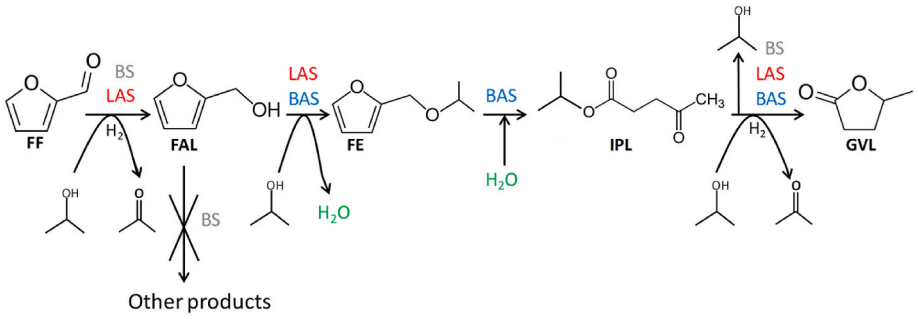

Scheme 1. Transformation of FF into GVL by hydrogenation. GVL: valerolactone; IPL: isopropyl levulinate; FE: furfuryl ether; FAL: furfuryl alcohol; LA: levulinic acid.

5 h and then a decrease took place. At long reaction times (8 and 12 h of reaction) the yield to FE decreased at the expense of GVL and other side products.

According to the results obtained in the present work and the knowledge from the literature [42,68,69], a reaction pathway for the formation of GVL from FF is proposed (Scheme 1). In this pathway, hydrogen can be obtained from 2-propanol as hydrogen donor. Initially, LAS together with weak basic sites can catalyze the hydrogenation of FF by MPV reduction to obtain FAL, which is subsequently etherified to furfural alcohol ether (FE). The transformation of FAL into FE can be catalyzed in the presence of LAS and BAS. Subsequently, FE can be transformed directly into IPL by ring opening, which apparently can be only carried out by BAS. Finally, IPL is transformed into GVL by hydrogenation via MPV reaction and a subsequent lactonization [15,49,68] in the presence of Lewis and weak basic sites.

To achieve an optimal GVL yield the presence of Lewis acid sites is essential. Nevertheless, the presence of small number of Brønsted acid sites and weak basic sites also facilitates the overall process. The highest catalytic activity was achieved by ZrO_2/Sep catalysts with a ZrO_2 loading of 9–17 wt%, which apart from having a suitable acidity/basicity and BAS/LAS ratios, showed well dispersed ZrO_2 particles on the support with prevalent weak basicity. The catalysts with low Zr-loading, i.e. 2.5ZrO_2/Sep presents ZrO_x species highly dispersed and tiny ZrO_2 nanoparticles. This is observed by TEM analysis and corroborated by the DR-UV-Vis data. Additionally, Zr-free sepiolite sites are also available for the substrate, which present low reactivity. In the case of the catalysts with 9–17 wt% Zr, well distributed zirconia particles are dispersed over the fibers of the sepiolite. In fact, the chemical analysis of different areas of the sample shows a highly homogeneous composition. However, if there is an excess of Zr, large bulk clusters are observed. In fact, for the 29ZrO_2/Sep catalyst, the DR-UV-Vis spectra show bands corresponding to isolated tetrahedral species but also to ZrO_2 clusters. This is in agreement with the heterogeneity in the particle distribution observed by TEM, in which two different areas with low and high Zr-loadings are observed. Therefore, high Zr-loadings should be avoided since the formation of bulk ZrO_2 (pure ZrO_2 shows a null capacity for the GVL formation) decreases the amount of active Zr-species dispersed on the sepiolite surface and as a consequence decreases the yield to GVL.

When Zr is deposited on a support, the ZrO_2 monolayer has been estimated to be $1.5748.10^{-3}$ g_{ZrO2} m^{-2}support [60]. Accordingly, in our study, the catalyst with 2.5% of ZrO_2 theoretically covers 10% of the surface support and therefore a large part of the support remains uncovered. The catalysts that have obtained the best performance (9–17 wt % ZrO_2) present an optimal coverage between 40 and 85%, whereas that catalyst with an excess of Zr (29ZrO_2/Sep) exceeds the theoretical monolayer (ca. 1.66 layers). This value is in agreement with the formation of bulk ZrO_2 without interacting with the support observed by different characterization techniques.

In order to know the stability of the optimal catalyst, a recycling test of 9ZrO_2/Sep was undertaken. The reaction was carried out five times

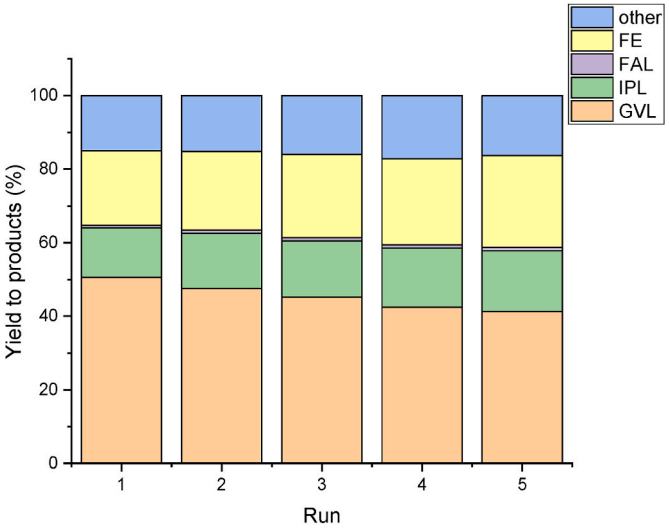

Fig. 9. Recycling test of 9ZrO_2/Sep in the production of GVL from FF with 2-propanol as hydrogen source. Reaction conditions: 0.25 mmol of FF in 5 mL of 2-propanol, 0.2 g of catalyst, for 5 h at 180 °C.

under identical conditions showing that the catalyst can be recycled but with a slight loss of activity after the first cycle (Fig. 9).

Finally, to investigate the ability of this catalytic system to selectively transform other compounds derived from the biomass, the catalyst 9ZrO_2/Sep was chosen and tested based on its optimum catalytic performance. The substrates used are levulinic acid (LA), methyl levulinate (ML) and ethyl levulinate (EL) (Table S1). In all cases, the substrate conversion was higher than 95% with yields to GVL of 88.4%, 92.3 and 88.3% from LA, ML and EL, respectively. The main by-product observed when LA was used as a substrate was IPL, which is produced by etherification with 2-propanol. On the other hand, the main by-product using EL and ML as substrates was LA, produced by alcoholysis. This preliminary study shows that 9ZrO_2/Sep could be efficient to produce GVL in high yields from other biomass-derived substrates using 2-propanol as a hydrogen donor.

5. Conclusions

γ-valerolactone can be efficiently obtained from furfural using 2-propanol as a solvent and as a hydrogen donor employing Zr supported on sepiolite catalysts, in spite of the fact that pure bulk ZrO_2 or pure sepiolite are unable to produce γ-valerolactone. In the present article, it has been shown that sepiolite, a cheap material directly obtained from a quarry, can be used as an effective support for the development of catalysts, which produce high yields to γ-valerolactone without the necessity of using more complex materials such as zeolites.

The optimal catalysts are those in which the Zr-support interaction is maximized, whereas the formation of bulk ZrO_2 must be avoided. This is achieved by catalysts with an intermediate Zr-content (between 9 and 17 wt% ZrO_2). Catalysts with ZrO_2 loadings higher than the theoretical monolayer are not suitable as they tend to form ZrO_2 aggregates. The formation of aggregated ZrO_2 has a negative impact in terms of catalytic performance since it inhibits the formation of γ-valerolactone and leads to fewer exposed Zr active sites with significant decrease in the intrinsic reactivity. According to the results obtained in the present work, the presence of Lewis acid sites is paramount for this reaction to take place selectively whereas low concentrations of Brønsted as well as basic sites can play a positive role. Interestingly, the optimal catalyst has been shown a reasonable level of stability keeping very similar catalytic activity after, at least, five catalytic runs.

Declaration of competing interest

The authors declare that they have no known competing financial interests or personal relationships that could have appeared to influence the work reported in this paper.

Data availability

Data will be made available on request.

Acknowledgments

A.G. thanks MINECO for the pre-doctoral grant (PRE2018-085211). This work was funded by the MAT2017-84118-C2-1-R, MAT2017-84118-C2-2-R, MCIN/AEI/10.13039/501100011033/projects and FEDER Una manera de hacer Europa. Authors thank the electron microscopy CAI center of UCM. Authors also thank the Generalitat Valenciana for CIAICO/2021/094.

Appendix A. Supplementary data

Supplementary data to this article can be found online at https://doi.org/10.1016/j.biombioe.2023.106730.

References

[1] J. Gu, J. Zhang, Y. Wang, D. Li, H. Huang, H. Yuan, Y. Chen, Efficient transfer hydrogenation of biomass derived furfural and levulinic acid via magnetic zirconium nanoparticles: experimental and kinetic stud, Ind. Crop. Prod. 145 (2020), 112133.
[2] S. Douvartzides, N.D. Charisiou, W. Wang, V.G. Papadakis, K. Polychronopoulou, M.A. Goula, Catalytic fast pyrolysis of agricultural residues and dedicated energy crops for the production of high energy density transportation biofuels. Part II: catalytic research, Renew. Energy 189 (2022) 315–338.
[3] D.R. Chaffey, T. Bere, T.E. Davies, D.C. Apperley, S.H. Taylor, A.E. Graham, Conversion of levulinic acid to levulinate ester biofuels by heterogeneous catalysts in the presence of acetals and ketals, Appl. Catal. B Environ. 293 (2021) 120219–120227.
[4] H. Chen, H. Ruan, X. Lu, J. Fu, T. Langrish, X. Lu, Catalytic conversion of furfural to methyl levulinate in a single-step route over Zr/SBA-15 in near-critical methanol, Chem. Eng. J. 333 (2018) 434–442.
[5] A. Guerrero-Torres, C.P. Jiménez-Gómez, J.A. Cecilia, C. García-Sancho, F. Franco, J.J. Quirante-Sánchez, P. Maireles-Torres, Ni supported on sepiolite catalysts for the hydrogenation of furfural to value-added chemicals: influence of the synthesis method on the catalytic performance, Top. Catal. 62 (2019) 535–550.
[6] F. Delbecq, Y. Wang, A. Muralidhara, K. El Ouardi, G. Marlair, C. Len, Hydrolysis of hemicellulose and derivatives—a review of recent advances in the production of furfural, Front. Chem. 6 (2018) 146.
[7] C. García-Sancho, C.P. Jiménez-Gómez, N. Viar-Antuñano, J.A. Cecilia, R. Moreno-Tost, J.M. Mérida-Robles, J. Requies, P. Maireles-Torres, Evaluation of the ZrO_2/Al_2O_3 system as catalysts in the catalytic transfer hydrogenation of furfural to obtain furfuryl alcohol, Appl. Catal. Gen. 609 (2021), 117905.
[8] O. He, Y. Zhang, P. Wang, L. Liu, Q. Wang, N. Yang, W. Li, P. Champagne, H. Yu, Experimental and kinetic study on the production of furfural and HMF from glucose, Catalysts 11 (2021) 11.
[9] G.W. Huber, S. Iborra, A. Corma, Synthesis of transportation fuels from biomass: chemistry, catalysts, and engineering, Chem. Rev. 106 (2006) 4044–4098.
[10] K. Yan, G. Wu, T. Lafleur, C. Jarvis, Production, properties and catalytic hydrogenation of furfural to fuel additives and value-added chemicals, Renew. Sustain. Energy Rev. 38 (2014) 663–676.
[11] L. Zhang, G. Xi, Z. Chen, D. Jiang, H. Yu, X. Wang, Highly selective conversion of glucose into furfural over modified zeolites, Chem. Eng. J. 307 (2017) 868–876.
[12] R. Mariscal, P. Maireles-Torres, M. Ojeda, I. Sádaba, M. L Granados, Furfural: a renewable and versatile platform molecule for the synthesis of chemicals and fuels, Energy Environ. Sci. 9 (2016) 1144–1189.
[13] L. Liu, H.M. Chang, H. Jameel, S. Park, Furfural production from biomass pretreatment hydrolysate using vapor-releasing reactor system, Bioresour. Technol. 252 (2018) 165–171.
[14] Y. Sun, Z. Wang, Y. Liu, X. Meng, J. Qu, C. Liu, B. Qu, A review on the transformation of furfural residue for value-added products, Energies 13 (2020) 21.
[15] K.D. Kim, J. Kim, W.Y. Teoh, J.C. Kim, J. Huang, R. Ryoo, Cascade reaction engineering on zirconia-supported mesoporous MFI zeolites with tunable Lewis–Brønsted acid sites: a case of the one-pot conversion of furfural to γ-valerolactone, RSC Adv. 10 (2020) 35318–35328.
[16] W. Gong, C. Chen, R. Fan, H. Zhang, G. Wang, H. Zhao, Transfer-hydrogenation of furfural and levulinic acid over supported copper catalyst, Fuel 231 (2018) 165–171.
[17] H. Wang, Y. Wu, Y. Li, J. Peng, X.K. Gu, M. Ding, One-step synthesis of gasoline fuels from γ-valerolactone with high selectivity over Cu/HZSM-5 bifunctional catalyst, Appl. Catal. B Environ. 296 (2021), 120338.
[18] J.Q. Bond, D.M. Alonso, D. Wang, R.M. West, J.A. Dumesic, Integrated catalytic conversion of γ-valerolactone to liquid alkenes for transportation fuels, Science 327 (2010) 1110–1114.
[19] D.M. Alonso, J.Q. Bond, J.C. Serrano-Ruiz, J.A. Dumesic, Production of liquid hydrocarbon transportation fuels by oligomerization of biomass-derived C 9 alkenes, Green Chem. 12 (2010) 992–999.
[20] A. García, R. Sanchis, P.J. Miguel, A.M. Dejoz, M.P. Pico, M.L. López, I. Álvarez-Serrano, T. García, B. Solsona, Low temperature conversion of levulinic acid into g-valerolactone using Zn to generate hydrogen from water and nickel catalysts supported on sepiolite, RSC Adv. 10 (2020) 20395–20404.
[21] J. He, H. Li, Y. Xu, S. Yang, Dual acidic mesoporous KIT silicates enable one-pot production of γ-valerolactone from biomass derivatives via cascade reactions, Renew. Energy 146 (2020) 359–370.
[22] T. Raj, K. Chandrasekhar, R. Banu, J.J. Yoon, G. Kumar, S.H. Kim, Synthesis of γ-valerolactone (GVL) and their applications for lignocellulosic deconstruction for sustainable green biorefineries, Fuel 303 (2021), 121333.
[23] X. Tang, X. Zeng, Z. Li, L. Hu, Y. Sun, S. Liu, T. Lei, L. Lin, Production of γ-valerolactone from lignocellulosic biomass for sustainable fuels and chemicals supply, Renew. Sustain. Energy Rev. 40 (2014) 608–620.
[24] S. Zhu, Y. Cen, J. Guo, J. Chai, J. Wang, W. Fan, One-pot conversion of furfural to alkyl levulinate over bifunctional Au-$H_4SiW_{12}O_{40}$/ZrO_2 without external H_2, Green Chem. 18 (2016) 5667–5675.
[25] T.M. Lima, C.G. Lima, A.K. Rathi, M.B. Gawande, J. Tucek, E.A. Urquieta-González, R. Zboril, M.W. Paixao, R.S. Varma, Magnetic ZSM-5 zeolite: a selective catalyst for the valorization of furfuryl alcohol to γ-valerolactone, alkyl levulinates or levulinic acid, Green Chem. 18 (2016) 5586–5593.
[26] K.L. MacIntosh, S.K. Beaumont, Nickel-catalysed vapour-phase hydrogenation of furfural, insights into reactivity and deactivation, Top. Catal. 63 (2020) 1446–1462.
[27] Z. Yu, X. Lu, C. Liu, Y. Han, N. Ji, Synthesis of γ-valerolactone from different biomass-derived feedstocks: recent advances on reaction mechanisms and catalytic systems, Renew. Sustain. Energy Rev. 112 (2019) 140–157.
[28] C. López-Aguado, M. Paniagua, J. Iglesias, G. Morales, J.L. García-Fierro, J. Melero A, Zr-USY zeolite: efficient catalyst for the transformation of xylose into bio-products, Catal. Today 304 (2018) 80–88.
[29] S. Nandi, A. Saha, P. Patel, N.U.H. Khan, R.I. Kureshy, A.B. Panda, Hydrogenation of furfural with nickel nanoparticles stabilized on nitrogen-rich carbon core–shell and its transformations for the synthesis of γ-Valerolactone in aqueous conditions, ACS Appl. Mater. Interfaces 10 (2018) 24480–24490.
[30] Q. Peng, H. Wang, Y. Xia, X. Liu, One-pot conversion of furfural to gamma-valerolactone in the presence of multifunctional zirconium alizarin red S hybrid, Appl. Catal. Gen. 621 (2021), 118203.
[31] H. Zhang, W. Yang, I.I. Roslan, S. Jaenicke, G.K. Chuah, A combo Zr-HY and Al-HY zeolite catalysts for the one-pot cascade transformation of biomass-derived furfural to γ-valerolactone, J. Catal. 375 (2019) 56–67.
[32] X. Gao, X. Yu, L. Peng, L. He, J. Zhang, Magnetic Fe_3O_4 nanoparticles and ZrO_2-doped mesoporous MCM-41 as a monolithic multifunctional catalyst for γ-valerolactone production directly from furfural, Fuel 300 (2021), 120996.
[33] L. Bui, H. Luo, W.R. Gunther, Y. Román-Leshkov, Domino reaction catalyzed by zeolites with Brønsted and Lewis acid sites for the production of γ-valerolactone from furfural, Angew. Chem. 125 (2013) 8180–8183.
[34] T. Wang, J. He, Y. Zhang, Production of γ-valerolactone from one-pot transformation of biomass-derived carbohydrates over chitosan-supported ruthenium catalyst combined with Zeolite ZSM-5, Eur. J. Org. Chem. 2020 (2020) 1611–1619.
[35] S. Song, L. Di, G. Wu, W. Dai, N. Guan, L. Li, Meso-Zr-Al-beta zeolite as a robust catalyst for cascade reactions in biomass valorization, Appl. Catal. B Environ. 205 (2017) 393–403.
[36] M. Koehle, R.F. Lobo, Lewis acidic zeolite Beta catalyst for the Meerwein–Ponndorf–Verley reduction of furfural, Catal. Sci. Technol. 6 (2016) 3018–3026.
[37] M.M. Antunes, S. Lima, P. Neves, A.L. Magalhães, E. Fazio, A. Fernandes, F. Neri, C. M. Silva, S.M. Rocha, M.F. Ribeiro, M. Pillinger, A. Urakawa, A.A. Valente, One-pot

conversion of furfural to useful bio-products in the presence of a Sn, Al-containing zeolite beta catalyst prepared via post-synthesis routes, J. Catal. 329 (2015) 522–537.
[38] J. Wang, K. Okumura, S. Jaenicke, G.K. Chuah, Post-synthesized zirconium-containing beta zeolite in meerwein–ponndorf–verley reduction: pros and cons, Appl. Catal. Gen. 493 (2015) 112–120.
[39] S. Zhu, Y. Xue, J. Guo, Y. Cen, J. Wang, W. Fan, Integrated conversion of hemicellulose and furfural into γ-valerolactone over Au/ZrO_2 catalyst combined with ZSM-5, ACS Catal. 6 (2016) 2035–2042.
[40] B. Hernández, J. Iglesias, G. Morales, M. Paniagua, C. López-Aguado, J.L. Garcia Fierro, P. Wolf, I. Hermans, J.A. Melero, One-pot cascade transformation of xylose into γ-valerolactone (GVL) over bifunctional Brønsted–Lewis Zr–Al-beta zeolite, Green Chem. 18 (2016) 5777–5781.
[41] J. Iglesias, J.A. Melero, G. Morales, M. Paniagua, B. Hernández, A. Osatiashtiani, A. F. Lee, K. Wilson, ZrO_2-SBA-15 catalysts for the one-pot cascade synthesis of GVL from furfural, Catal. Sci. Technol. 8 (2018) 4485–4493.
[42] J.A. Melero, G. Morales, J. Iglesias, M. Paniagua, C. López-Aguado, Rational optimization of reaction conditions for the one-pot transformation of furfural to γ-valerolactone over Zr–Al-beta zeolite: toward the efficient utilization of biomass, Ind. Eng. Chem. Res. 57 (2018) 11592–11599.
[43] H.P. Winoto, Z.A. Fikri, J.M. Ha, Y.K. Park, H. Lee, D.J. Suh, J. Jae, Heteropolyacid supported on Zr-Beta zeolite as an active catalyst for one-pot transformation of furfural to γ-valerolactone, Appl. Catal. B Environ. 241 (2019) 588–597.
[44] L. Ye, Y. Han, H. Bai, X. Lu, HZ-ZrP catalysts with adjustable ratio of Brønsted and Lewis acids for the one-pot value-added conversion of biomass-derived furfural, ACS Sustain. Chem. Eng. 8 (2020) 7403–7413.
[45] C. Zhou, Y. Xiao, S. Xu, J. Li, C. Hu, γ-valerolactone production from furfural residue with formic acid as the sole hydrogen resource via an integrated strategy on Au-Ni/ZrO_2, Ind. Eng. Chem. Res. 59 (2020) 17228–17238.
[46] S. Morandi, M. Manzoli, C.E. Chan-Thaw, B. Bonelli, M. Stucchi, L. Prati, H. Stormer, W. Wang, D. Wang, M. Pabel, A. Villa, Unraveling the effect of ZrO_2 modifiers on the nature of active sites on AuRu/ZrO_2 catalysts for furfural hydrogenation, Sustain. Energy Fuels 4 (2020) 1469–1480.
[47] H.P. Winoto, B.S. Ahn, J. Jae, Production of γ-valerolactone from furfural by a single-step process using Sn-Al-Beta zeolites: optimizing the catalyst acid properties and process conditions, J. Ind. Eng. Chem. 40 (2016) 62–71.
[48] G. Yu, H. Ma, J. Wang, S. Qin, Z. Yang, Y. Li, Highly flexible and active potassium-supported sepiolite paper catalysts for soot oxidation, Catal. Sci. Technol. 10 (2020) 1875–1880.
[49] B.S. Rao, P.K. Kumari, P. Koley, J. Tardio, N. Lingaiah, One pot selective conversion of furfural to γ-valerolactone over zirconia containing heteropoly tungstate supported on β-zeolite catalyst, Mol. Catal. 466 (2019) 52–59.
[50] E.P. Parry, An infrared study of pyridine adsorbed on acidic solids. Characterization of surface acidity, J. Catal. 2 (1963) 371–379.
[51] M. Saito, T. Aihara, H. Miura, T. Shishido, Brønsted acid property of alumina-based mixed-oxides-supported tungsten oxide, Catal. Today 375 (2021) 64–69.
[52] A. García, R. Sanchis, F.J. Llopis, I. Vázquez, M.P. Pico, M.L. López, I. Álvarez-Serrano, B. Solsona, Ni supported on natural clays as a catalyst for the transformation of levulinic acid into γ-valerolactone without the addition of molecular hydrogen, Energies 13 (2020) 3448.
[53] P.R. Rauta, P. Manivasakan, V. Rajendran, B.B. Sahu, B.K. Panda, P. Mohapatra, Phase transformation of ZrO_2 nanoparticles produced from zircon, Phase Transitions 85 (2012) 13–26.
[54] D. Karataş, D. Senol Arslan, I. Kursun Unver, O. Ozdemir, Coating mechanism of AuNPs onto sepiolite by experimental research and MD simulation, Coatings 9 (2019) 785.
[55] A. Ongen, H.K. Ozcan, E.E. Ozbas, N. Balkaya, Adsorption of Astrazon Blue FGRL onto sepiolite from aqueous solutions, Desalination Water Treat. 40 (2012) 129–136.
[56] S. Lazarević, I. Janković-Častvan, D. Jovanović, S. Milonjić, D. Janaćković, R. Petrović, Adsorption of Pb^{2+}, Cd^{2+} and Sr^{2+} ions onto natural and acid-activated sepiolites, Appl. Clay Sci. 37 (2007) 47–57.
[57] A.A. Elmadani, I. Radović, N.Z. Tomić, M. Petrović, D.B. Stojanović, R. J. Heinemann, V. Radojević, Hybrid denture acrylic composites with nanozirconia and electrospun polystyrene fibers, PLoS One 14 (2019), e0226528.
[58] X. Li, X. Yuan, G. Xia, J. Liang, C. Liu, Z. Wang, W. Yang, Catalytic production of γ-valerolactone from xylose over delaminated Zr-Al-SCM-1 zeolite via a cascade process, J. Catal. 392 (2020) 175–185.
[59] A. Ramanathan, M.C. Castro Villalobos, C. Kwakernaak, S. Telalovic, U. Hanefeld, Zr-TUD-1: a Lewis acidic, three-dimensional, mesoporous, zirconium-containing catalyst, Chem. Eur J. 14 (2008) 961–972.
[60] T. Horiuchi, Y. Teshima, T. Osaki, T. Sugiyama, K. Suzuki, T. Mori, Improvement of thermal stability of alumina by addition of zirconia, Catal. Lett. 62 (1999) 107–111.
[61] C. Colbea, D. Avram, B. Cojocaru, R. Negrea, C. Ghica, V.G. Kessler, G. A. Seisenbaeva, V. Parvulescu, C. Tiseanu, Full tetragonal phase stabilization in ZrO_2 nanoparticles using wet impregnation: interplay of host structure, dopant concentration and sensitivity of characterization technique, Nanomaterials 8 (2018) 988.
[62] M.A. Gondal, T.A. Fasasi, U. Baig, A. Mekki, Effects of oxidizing media on the composition, morphology and optical properties of colloidal zirconium oxide nanoparticles synthesized via pulsed laser ablation in liquid technique, J. Nanosci. Nanotechnol. 18 (2018) 4030–4039.
[63] A. García, P.J. Miguel, A. Ventimiglia, N. Dimitratos, B. Solsona, Optimization of the Zr-loading on siliceous support catalysts leads to a suitable Lewis/Brønsted acid sites ratio to produce high yields to γ-valerolactone from furfural in one-pot, Fuel 324 (2022), 124549.
[64] Y. Shao, Q. Li, X. Dong, J. Wang, K. Sun, L. Zhang, S. Zhang, L. Xu, X. Yuan, X. Hu, Cooperation between hydrogenation and acidic sites in Cu-based catalyst for selective conversion of furfural to γ-valerolactone, Fuel 293 (2021), 120457.
[65] D. Li, J. Zhang, Y. Liu, H. Yuan, Y. Chen, Boron doped magnetic catalysts for selective transfer hydrogenation of furfural into furfuryl alcohol, Chem. Eng. Sci. 229 (2021), 116075.
[66] H. Li, Z. Fang, S. Yang, Direct conversion of sugars and ethyl levulinate into γ-valerolactone with superparamagnetic acid–base bifunctional $ZrFeO_x$ nanocatalysts, ACS Sustain. Chem. Eng. 4 (2016) 236–246.
[67] X. Tang, H. Chen, L. Hu, W. Hao, Y. Sun, X. Zeng, L. Lin, S. Liu, Conversion of biomass to γ-valerolactone by catalytic transfer hydrogenation of ethyl levulinate over metal hydroxides, Appl. Catal. B Environ. 147 (2014) 827–834.
[68] R. Maderuelo-Solera, S. Richter, C.P. Jiménez-Gómez, C. García-Sancho, F. J. García-Mateos, J.M. Rosas, R. Moreno-Tost, J.A. Cecilia, P. Maireles-Torres, Porous SiO_2 nanospheres modified with ZrO_2 and their use in one-pot catalytic processes to obtain value-added chemicals from furfural, Ind. Eng. Chem. Res. 60 (2021) 18791–18805.
[69] W. Li, Z. Cai, H. Li, Y. Shen, Y. Zhu, H. Li, X. Zhang, F. Wang, Hf-based metal organic frameworks as bifunctional catalysts for the one-pot conversion of furfural to γ-valerolactone, Mol. Catal. 472 (2019) 17–26.